Received: 17 March 2018 | Accepted: 11 June 2018

DOI: 10.1111/jace.15876

ORIGINAL ARTICLE

Journal of the American Ceramic Society

Effect of additive structure and size on SiO_2 formation in polymer-derived SiOC ceramics

Donald Erb | **Kathy Lu***

Department of Materials Science and Engineering, Virginia Polytechnic Institute and State University, Blacksburg, Virginia

Correspondence
Kathy Lu, Department of Materials Science and Engineering, Virginia Polytechnic Institute and State University, Blacksburg, VA.
Email: klu@vt.edu

Funding information
Division of Civil, Mechanical and Manufacturing Innovation, Grant/Award Number: NSF CMMI-1634325

Abstract

Silicon oxycarbide (SiOC) ceramics with highly adjustable properties and microstructures have many promising applications in batteries, catalysis, gas separation, and supercapacitors. In this study, additive structures on the nucleation and growth of SiO_2 within SiOC ceramics are investigated by adding cyclic tetramethyl-tetravinylcyclotetrasiloxane (TMTVS) or caged octavinyl-polyhedral oligomeric silsesquioxane (POSS) to a base polysiloxane (PSO) precursor. The effects of the 2 additives on the polymer-to-ceramic transformation and the phase formation within the SiOC are discussed. POSS encourages SiO_2 nucleation and leads to more SiO_2 formation with significantly increased ceramic yield, which subsequently leads to higher specific surface of 1557 m^2/g with a larger pore size of ~1.8 nm for the porous SiOC. High TMTVS content decreases both the specific surface area and pore volume of the resulting porous SiOCs. This study demonstrates a new approach of using Si-rich additive POSS to increase the SiOC yield while maintaining or even increasing the specific surface area.

KEYWORDS
polyhedral oligomeric silsesquioxane, polymer-derived ceramic, pores/porosity, Silicon oxycarbide

1 | INTRODUCTION

Polymer-derived ceramics, such as SiOC, SiCN, and SiBCN, offer exciting properties because the microstructures and compositions of the ceramic materials can be controlled on the molecular level by focusing on the cross-linking and pyrolysis of the polymer precursors.[1–3] In particular, silicon oxycarbide, SiOC, in both bulk and porous forms, has great application potential in batteries, catalysis, gas separation, and supercapacitors due to its high-temperature stability, resistance to devitrification, and oxidation resistance.[1,4] After pyrolysis of the preceramic polymer, SiOC is composed of mixed SiO_xC_{4-x} bonds ($0 < x < 4$). Upon further heating to temperatures above 1000°C, SiO_2 and free carbon phases form in the SiOC matrix; at temperatures above approximately 1300°C, the SiOC matrix further phase separates into additional SiO_2 and carbon, as well as SiC nanocrystals.[2,5,6] The formation temperature and content of each of the phases can be controlled by tailoring the polymer precursors and pyrolysis conditions.[6–10] However, the ceramic yield is generally ≤70% and severely limits the practical uses.

Several studies have been conducted on the effect of the polymer precursor architectures (e.g., linear, cyclic, cage) on the phase formation within the SiOC after pyrolysis. The effect of using a cyclic precursor, tetramethyl cyclotetrasiloxane (TMTS), vs a linear precursor, polyhydromethylsiloxane (PHMS), was investigated using either tetramethyl-tetravinylcyclotetrasiloxane (TMTVS)[11] or divinylbenzene[12,13] as a cross-linking agent. The cyclic TMTS resulted in the formation of both crystalline and amorphous SiO_2 whereas the linear PHMS only led to amorphous SiO_2 after pyrolysis at 1400°C. For the effects of caged molecules on the pyrolysis of polymers, several

*Member, American Ceramic Society

 © 2018 The American Ceramic Society

studies added polyhedral oligomeric silsesquioxane (POSS) to polymer precursors for fabricating SiOC, but the pyrolysis temperatures in these studies were limited to <1100°C.[14–17] In addition, the phase formation within the POSS-derived SiOC ceramics has not been well studied. Thus, further investigation on the effects of the POSS cage structure on the phase formation in SiOC ceramics is needed.

The formation of the SiO_2 phase within SiOC ceramics has been shown to be highly dependent on the size of the additive. A SiO_2 powder with an average size between 15 and 20 nm was added to a polysiloxane (PSO) and pyrolyzed. The addition of the SiO_2 caused an increase in pore volume after etching with hydrofluoric acid. However, the samples with the added SiO_2 powder also had a greater volume of pores (<10 nm in size), which could not be attributed to the added powder but rather to more extensive phase separation of the SiOC phase.[18] 10 wt% of either tetramethyl orthosilicate (TMOS) or tetraethyl orthosilicate (TEOS) was added to a base PSO and in situ hydrolyzed using water vapor injection during pyrolysis.[19] Both the TMOS and TEOS decreased the pore size after etching relative to the PSO sample, but the TMOS significantly decreased the specific surface area while the addition of TEOS increased the specific surface area. The difference in the behaviors of the 2 additives was attributed to the size difference, with the TMOS not forming large enough SiO_2 nuclei but instead forming amorphous, HF-unetchable SiOC.[19] Thus, the size of the additive responsible for SiO_2 formation in SiOC must be properly controlled to influence the SiOC characteristics, such as yield, pore size, specific surface area, etc.

In this work, microporous SiOC ceramics are fabricated through the addition of either TMTVS or polyhedral oligomeric silsesquioxane (POSS) to a polysiloxane-based precursor in order to investigate the effect of the additives on the formation of SiO_2 nanodomains after pyrolysis. The precursors are pyrolyzed in a water vapor atmosphere, which encourages the formation of SiO_2 within the SiOC ceramics.[8,9,19,20] After pyrolysis, SiO_2 nanoclusters are etched with a HF solution to create single nanometer pores, with the ultimate goal being to fabricate porous SiOC ceramics with high surface areas. The effects of the additive size, amount, and pyrolysis temperature on the resulting thermophysical properties, phase evolution, specific surface area, and pores of the SiOC ceramics are studied.

2 | EXPERIMENTAL PROCEDURES

A commercial polysiloxane (PSO, $[-Si(C_6H_5)_2O-]_3[-Si(CH_3)(H)O-]_2[-Si(CH_3)(CH=CH_2)O-]_2$, SPR-684, Starfire Systems, Inc., Gelest Inc., Schenectady, NY) was chosen as the base polymer and 2.1%-2.4% platinum-divinyltetramethyldisiloxane complex in xylene (Pt catalyst, Gelest Inc., Morrisville, PA) was used as the catalyst. 2,4,6,8-tetramethyl-2,4,6,8-tetravinylcyclotetrasiloxane (TMTVS, 97%, Fisher Scientific, Pittsburgh, PA) and octavinyl-polyhedral oligomeric silsesquioxane (POSS, OL1170, Hybrid Plastics, Hattiesburg, MS) were used as additives in the base PSO, and acetone (HPLC grade, Fisher Scientific, Pittsburgh, PA) was used as the solvent.

For the solutions with TMTVS additions, PSO and TMTVS were mixed with either 0, 10, 20, 30, or 40 wt% TMTVS. Adequate acetone was added to reduce the viscosity of the solution, having approximate volume ratios of 0.2:0.8 acetone to PSO+TMTVS. The mixtures were sonicated for 10 minutes and then mixed in a high-energy ball mill (SPEX 8000M Mixer/Mill, SPEX SamplePrep, Metuchen, NJ) for 10 minutes to form a homogeneous mixture. Next, the Pt catalyst (1 wt% relative to PSO) was added, the mixtures were mixed again in a high-energy ball mill for 5 minutes, and then poured into aluminum foil molds. For the solutions containing POSS, additional acetone was used to fully dissolve POSS before mixing with the PSO; the acetone to POSS volume ratio was 5:1. PSO was then added to the solution to make 10, 20, 30, and 40 wt% POSS mixtures. All other preparation steps for the POSS mixtures were the same as for TMTVS.

Once transferred to the molds, the mixtures were placed into a vacuum chamber and vacuumed for 30 minutes at approximately 20 Torr to remove all the solvent and any bubbles from the solutions. After that, the molds were put in an oven to cross-link at 50°C for 12 hours and then at 120°C for 6 hours. The samples designated as PSO correspond to the pure PSO sample; the samples with POSS or TMTVS were labeled as XP or XT, respectively, where X is the weight percent of POSS or TMTVS.

To prepare the samples for pyrolysis, the cross-linked materials were first cut and polished into circular pieces roughly 10 mm in diameter and 2 mm in thickness. Next, the samples were placed into a zirconia crucible, covered on both sides with graphite mats in order to reduce friction during shrinkage and prevent warping,[21,22] and put into a tube furnace (1730-20 Horizontal Tube Furnace, CM Furnaces Inc., Bloomfield, NJ). With an Ar flow rate of about 500 std cm^3/min, the samples were heated up to 1100°C, 1300°C, or 1400°C at a rate of 1°C/min, held for 2 hours, cooled to 400°C with a rate of 1°C/min, and finally cooled to 50°C with a rate of 2°C/min. During heating from 500°C-700°C, the Ar was bubbled through water at 60°C, giving a gas flow with a Ar:H_2O molar ratio of approximately 5:1. The purpose of the water vapor injection was to facilitate the formation of Si–O bonds and remove free C within the samples in order to encourage SiO_2 nucleation at higher temperatures.[8,9,19,20]

Etching of the bulk SiOC samples after pyrolysis was done using a HF solution (20 wt% HF in water), which was magnetically stirred at room temperature until no significant mass loss was detected for the samples, taking approximately 4 days. The SiOC samples were then rinsed with deionized water and dried at 120°C. The mass loss due to etching was calculated by dividing the change in mass after etching by the original mass.

Ceramic yield was calculated by measuring the mass of the samples before and after the pyrolysis. The chemical bonding was evaluated using Fourier Transform Infrared Spectroscopy (FT-IR) (Nicolet 8700 with Pike GladiATR attachment, Thermo Scientific, Waltham, MA) between 500 and 4000 cm^{-1} wave number with a resolution of 4 cm^{-1} and averaged between 64 scans. The thermal decomposition of the polymers was investigated by thermogravimetric analysis (TGA) using a STA 449C Jupiter® analyzer (Netzsch-Gerätebau GmbH, Selb, Germany) from room temperature to 1000°C with a heating rate of 5°C/min and a N_2 flux of 40 mL/min. The densities of the bulk samples were measured using a pycnometer (AccuPyc II 1340, Micromeritics, Norcross, GA) with high purity helium gas. The phase compositions of the pyrolyzed samples were analyzed in an X'Pert PRO diffractometer (PANalytical B.V., EA Almelo, the Netherlands) with Cu Kα radiation. The JCPDS reference cards used to identify the crystalline phases were 00-039-1425 for SiO_2, 00-029-1129 for SiC, and 01-075-1621 for C. The specific surface area, pore size distribution, and pore volume of the pyrolyzed samples were evaluated using nitrogen adsorption at 77 K with a Quantachrome Autosorb-1 (Quantachrome Instruments, Boynton Beach, FL), and the samples were degassed before testing for 3 hours at 300°C. The pore size distribution and pore volume were derived by applying the Non Local Density Functional Theory (NLDFT) to the adsorption branch of the data.[23] Assuming cylindrical pores, the average pore size was estimated using 4000 V/A, where V was the pore volume and A was the specific surface area.[24]

3 | RESULTS AND DISCUSSION

3.1 | Polymer architecture and bonding

The PSO, TMTVS, and POSS species have distinct differences in their molecular structures; PSO is composed of linear polymer chains, TMTVS has a cyclic structure, and POSS has a cage-like structure, as shown in Figure 1A-C. Previous studies have shown that polymer precursors containing more cyclic structures favor the formation of larger SiO_2 nuclei during pyrolysis,[12] so determining the architecture of the Si–O–Si bonds within the precursor is significant. The differences in the architecture of organosilicon species can be determined by the position of the FT-IR Si–O–Si peak at 1000-1100 cm^{-1} wave number (Figure 1D). For long polymer chains, such as PSO, the Si–O–Si bond displays a broad peak between ~1000 cm^{-1} and 1100 cm^{-1} wave number. For cyclic molecules with less than ~ 20 siloxane repeat units, such as TMTVS, the Si–O–Si peak position is well-defined and centered at ~1050 cm^{-1} wave number. Likewise, for siloxanes with a cage structure, such as POSS, the peak is also well-defined and centered at ~1100 cm^{-1} wave number.[17,25] The integration of the additives into the PSO causes new peaks to appear at 1050 cm^{-1} or 1100 cm^{-1} wave number due to the different architectures of the additives (Figure 1D).

Figure 1C also shows the presence of residual vinyl bonds for the samples with TMTVS and POSS additions. For the base PSO, cross-linking occurs through hydrosilylation between the hydrogen and vinyl groups, which are present in equal molar amounts in the PSO. The consumption of the hydrogen bonds is evident in Figure 1D comparing the spectra of the pure PSO before cross-linking (PSO-Pre) and after, which shows the disappearance of the Si–H absorption peak near 2160 cm^{-1} wave number.[26] With the addition of either TMTVS or POSS to PSO, additional vinyl bonds are added to the polymer, leaving unreacted vinyl groups after cross-linking, as seen by the absorption peaks at 1405 cm^{-1} and 1604 cm^{-1} wave number for the 30T and 30P samples.[17] The theoretical molar ratios of vinyl to hydrogen groups for the POSS samples are 1.6, 2.4, 3.4, and 4.7 for the 10P, 20P, 30P, and 40P samples, respectively. For the TMTVS samples, the theoretical molar ratios of vinyl to hydrogen groups is 1.6, 2.3, 3.2, and 4.4, for the 10T, 20T, 30T, and 40T samples, respectively. The residual vinyl bonds for both the TMTVS and POSS may have an effect on the bond formation during pyrolysis because the vinyl bonds can react with either other vinyl bonds or methyl bonds at elevated temperatures.[27]

3.2 | Thermophysical properties

Analysis of the thermal decomposition behavior for the PSO, 30T, and 30P samples up to 1000°C was conducted using TGA as shown in Figure 2. Since the TGA was conducted in inert nitrogen while the actual samples were fabricated with water vapor injection between 500°C and 700°C, the focus of the TGA results will be for the initial decomposition of the precursors at temperatures below 500°C. The pure PSO sample shows 2 major mass loss steps at 400°C and 550°C. The mass loss at 400°C is associated with depolymerization of the siloxane chains resulting in the formation of volatile cyclic siloxane molecules,

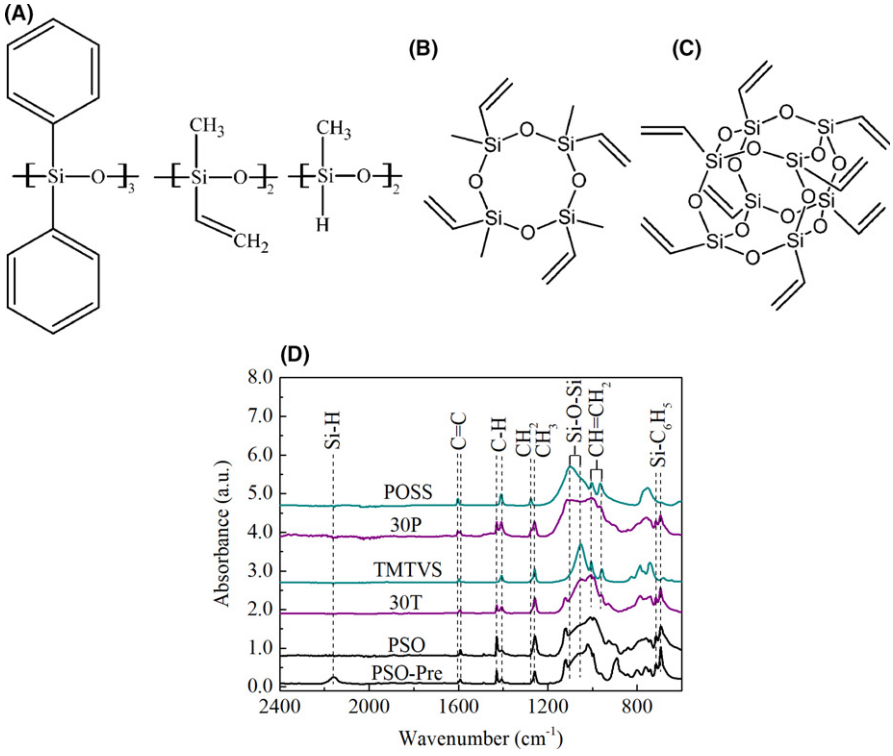

FIGURE 1 Chemical structures of (A) PSO, (B) TMTVS, and (C) POSS, and (D) the FT-IR absorption spectra for the PSO before cross-linking (PSO-Pre) and the cross-linked PSO, 30T, and 30P polymers, as well as pure TMTVS and POSS [Color figure can be viewed at wileyonlinelibrary.com]

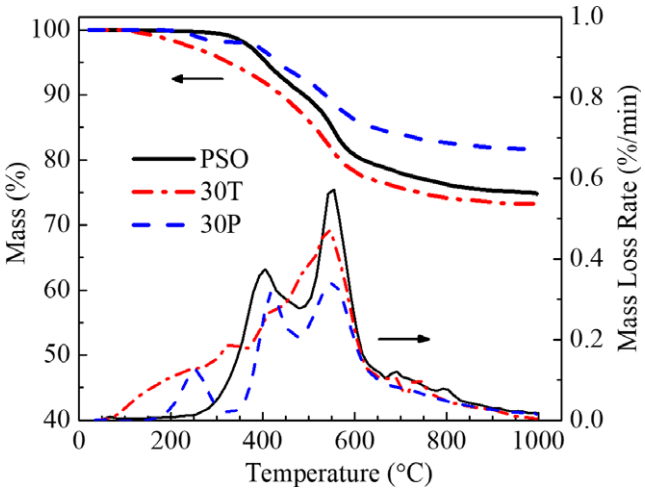

FIGURE 2 TG and dTG for the PSO, 30T, and 30P samples in nitrogen [Color figure can be viewed at wileyonlinelibrary.com]

and the mass loss at 550°C is attributed to the release of various hydrocarbon compounds.[28,29] The 30T sample, however, displays continuous degradation beginning at approximately 100°C due to the evaporation of TMTVS, which has a boiling temperature of ~110°C. The mass loss rate for the 30T sample continuously increases until reaching a maximum at 500°C. For the 30P sample, there are two well-defined maxima in the mass loss rate at 400°C and 550°C, similar to the PSO, as well as a third maxima at 250°C; the peak at 250°C corresponds to the decomposition of the POSS molecules.[16] However, the mass loss after the 250°C degradation step is <2%; the majority of the POSS added to the polymer remains in the polymer precursor during further heating.

The ceramic yield and linear shrinkage of the polymers after pyrolysis at 1100°C is shown in Figure 3A. The yield for the 10T and 20T samples is slightly greater than for the pure PSO sample, increasing from 72.2% for PSO to 74.1% for 20T. The increase in the ceramic yield may be due to a higher cross-linking density with the incorporation of up to 20 wt% TMTVS as well as the lower hydrocarbon content of TMTVS compared with the base PSO. With the addition of more TMTVS, however, the yield decreases to 70.9% for 30T and 66.6% for 40T, likely because the TMTVS is not fully incorporated into the PSO matrix and thus evaporates or decomposes to a greater extent during pyrolysis. The TG and dTG data for the 20T sample confirmed this (Figure S1), with the 20T sample showing less mass loss at temperatures lower than 300°C compared with the 30T sample. For the samples with POSS, the ceramic yield continually increases as the amount of POSS increases, from 74.7% for 10P to 82.3% for 40P. The thermal stability enhancement for octavinyl-POSS has been shown in POSS-PDMS systems.[16] Similar to the TMTVS, this increase in yield may be due to an increase in the cross-linking density with more POSS. In addition, the residual vinyl bonds in the POSS samples may react with either other vinyl groups or methyl groups during pyrolysis, creating additional linkages and

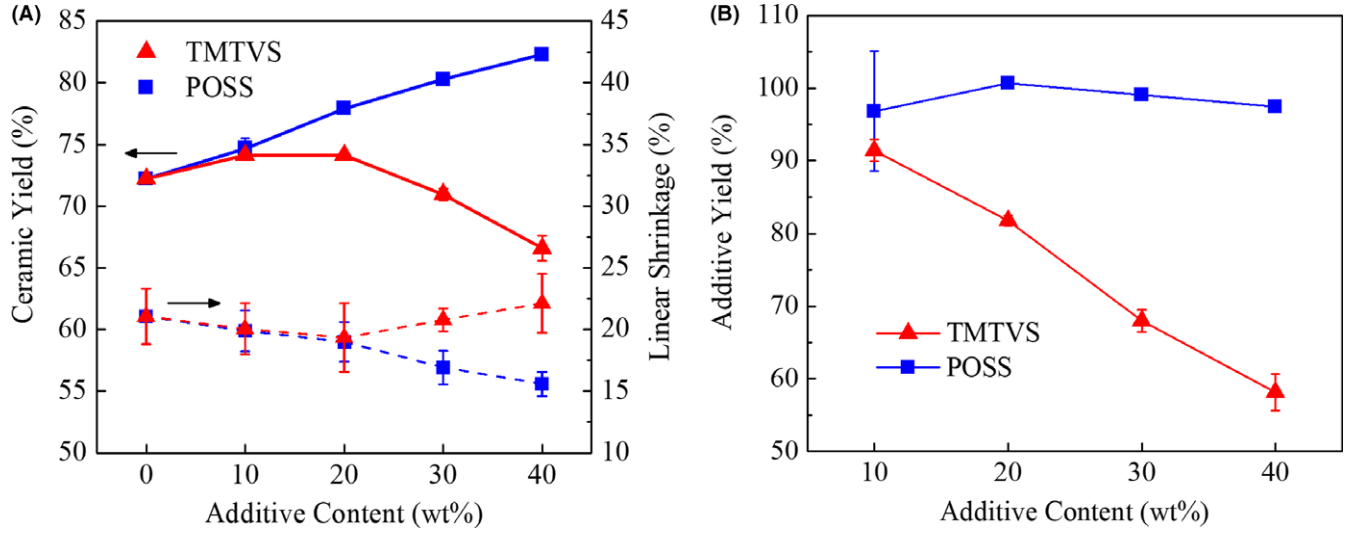

FIGURE 3 (A) Ceramic yield and linear shrinkage of the PSO sample with the TMTVS and POSS additives after pyrolysis at 1100°C, and (B) yield of the TMTVS and POSS additives as a function of content within the PSO precursor after pyrolysis at 1100°C [Color figure can be viewed at wileyonlinelibrary.com]

further improving the thermal stability and thus yield.[30] This 14% yield increase vs the PSO sample is especially significant to large-scale applications.

From Figure 3A, it is apparent that the additives have a significant influence on the ceramic yield of the polymer precursors. Assuming that the additive does not have a compounding effect within the polymer blends to influence the yield of the PSO, the ceramic yield of the additive, y_f, is given by:

$$y_f = \frac{Y - y_{PSO}(1 - x_f)}{x_f} \quad (1)$$

where Y is the measured ceramic yield of the polymer precursors in Figure 3A, y_{PSO} is the yield of the pure PSO sample, and x_f is the mass fraction of the additive in the polymer. The standard deviation for Equation (1), σ_{y_f}, can be obtained using propagation of uncertainty[31]:

$$_{y_f} = \frac{\sqrt{[\sigma_Y]^2 + [\sigma_{y_{PSO}}(1 - x_f)]^2}}{x_f} \quad (2)$$

where σ_Y is the standard deviation of the measured ceramic yield and $\sigma_{y_{PSO}}$ is the standard deviation of the yield of the PSO sample. Applying Equations (1) and (2) to the measured ceramic yields for the samples pyrolyzed at 1100°C leads to Figure 3B. For TMTVS, the additive yield continuously decreases as the content within the polymer is increased, changing from 91.4% for 10T to 58.1% for 40T. The POSS additive leads to very little change between the different samples, going from 96.8% for 10P to 97.5% for 40P; the calculated yield is consistent with the TGA results for the 30P sample, which only experiences a mass loss of about 2% near the sublimation temperature of POSS, 250°C.

The calculated additive yield for POSS is consistent with previous studies and is due to 2 factors: the size of the POSS molecules and the unreacted vinyl bonds. Yang et al[16] showed that POSS with either phenyl or vinyl functional groups was physically mixed with polydimethylsiloxane and both POSS types improved the thermal stability due to lowering the mobility of the siloxane chains and the kinetics of the chain scission. The POSS with the vinyl functional group, however, had a ceramic yield twice that of the phenyl POSS due to the vinyl groups causing further reactions during pyrolysis and strengthening the polymer network.[16] This same improvement from the vinyl bonds is seen for the 10T and 20T samples, but the addition of more TMTVS causes partial evaporation before the temperatures are high enough for the vinyl bonds to react. Thus, the higher TMTVS contents lead to lower yields.

The linear shrinkage for the TMTVS-containing samples, as shown in Figure 3A, initially decreases from 21.1% for PSO to 19.3% for the 20T sample, but then increases with further addition of TMTVS, reaching 22.1% for the 40T sample. Overall, the linear shrinkage is not greatly affected by the amount of TMTVS within the polymer precursor, especially when considering the standard deviations of the measurements as shown in Figure 3A. The addition of the POSS causes a continual and consistent decrease in linear shrinkage, from 19.9% for the 10P sample to 15.6% for the 40P sample. Understandably, the linear shrinkage trend for the POSS samples is opposite to the ceramic yield trend.

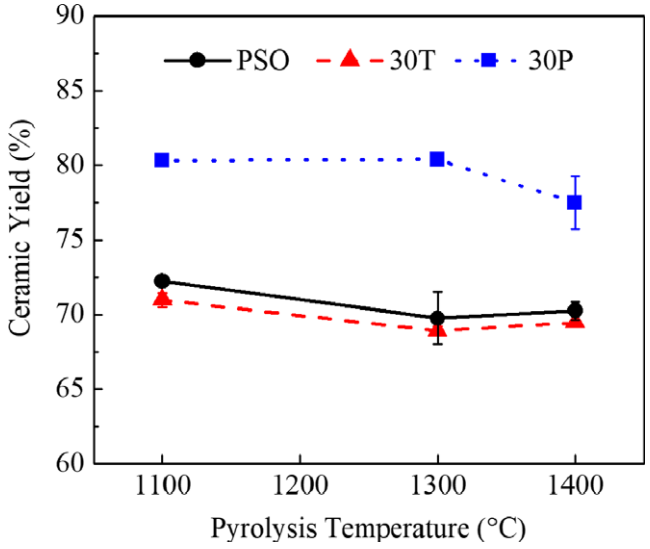

FIGURE 4 Ceramic yield of PSO, 30T, and 30P at various pyrolysis temperatures [Color figure can be viewed at wileyonlinelibrary.com]

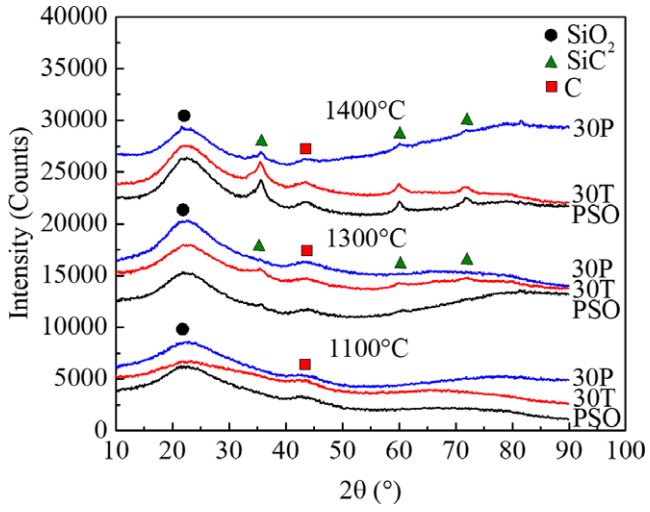

FIGURE 5 XRD patterns for the PSO, 30T, and 30P samples pyrolyzed at 1100°C, 1300°C, and 1400°C [Color figure can be viewed at wileyonlinelibrary.com]

The yields of the PSO, 30P, and 30T samples after pyrolysis at 1100°C, 1300°C, and 1400°C are shown in Figure 4. The yield for the pure PSO sample decreases slightly between 1100°C and 1300°C, from 72.2% to 70.2%, likely due to the carbothermal reduction of SiO_2 to be discussed later, and is consistent with previous studies using the same PSO precursor.[9,18] The ceramic yield for the PSO sample is then nearly the same between 1300°C and 1400°C, suggesting that there is no further carbothermal reduction. The 30T sample shows a similar trend as the PSO sample, with the major mass loss step being between 1100°C and 1300°C. For the 30P sample, the slight mass loss is delayed to higher temperatures between

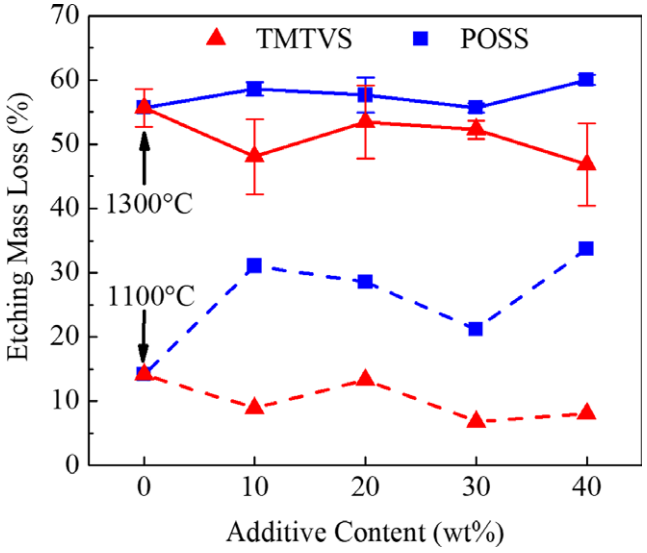

FIGURE 6 Mass loss after HF etching of the samples pyrolyzed at 1100°C (dashed lines) and 1300°C (solid lines) [Color figure can be viewed at wileyonlinelibrary.com]

1300°C and 1400°C, demonstrating the enhanced stability of the SiOC system with the POSS addition, but is of similar magnitude as those observed for the PSO and 30T samples. For the other TMTVS and POSS samples, the correlation between the yield and pyrolysis temperature is similar as discussed for the 30T and 30P samples.

The density of the PSO sample after pyrolysis at 1100°C is 1.90 g/cm^3, lower than that of typical SiOC systems (density ~ 2.3 g/cm^3),[32–34] due to the significant amount of turbostratic carbon (density ~1.45 g/cm^3) present in the sample.[22] For the POSS samples, the densities are 1.90 g/cm^3, 1.91 g/cm^3, 1.87 g/cm^3, and 1.87 g/cm^3 for 10P, 20P, 30P, and 40P, respectively. Likewise, the densities for 10T, 20T, 30T, and 40T samples are 1.91 g/cm^3, 1.91 g/cm^3, 1.93 g/cm^3, and 1.91 g/cm^3, respectively. Thus, neither the TMTVS nor POSS additives influence the bulk density, which can be understood by considering the yield and shrinkage trends shown in Figure 3A. For both additives, the ceramic yield and linear shrinkage show inverse trends, which result in similar densities for all the samples after pyrolysis.

3.3 | Phase evolution

All of the samples after pyrolysis at 1100°C are amorphous, as shown in Figure 5, with diffraction peaks only for turbostratic carbon at 43° and a broad peak centered around 23° for amorphous SiO_2. At a higher pyrolysis temperature of 1300°C, the samples still display the turbostratic carbon peak at 43° and a strong amorphous SiO_2 peak. In addition, small broad peaks at 35.6°, 60°, and 72° begin to appear for the PSO and 30T samples, indicating the formation of nanocrystalline β–SiC. The SiC formation is more evident for the samples with higher TMTVS

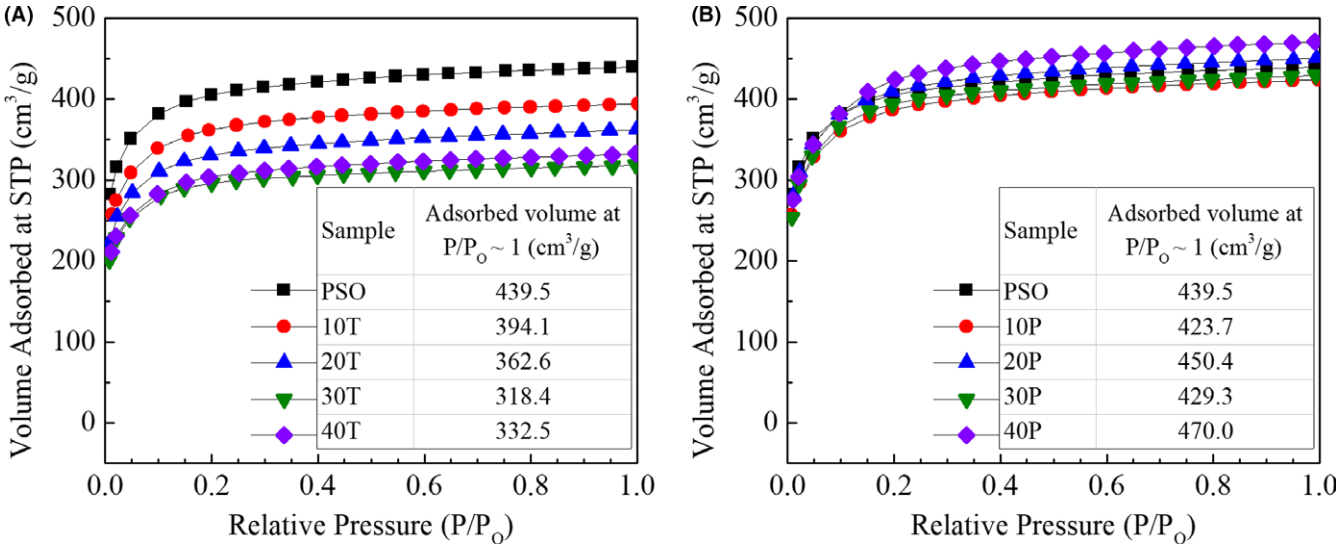

FIGURE 7 Nitrogen adsorption isotherms for (A) TMTVS and (B) POSS samples pyrolyzed at 1300°C [Color figure can be viewed at wile yonlinelibrary.com]

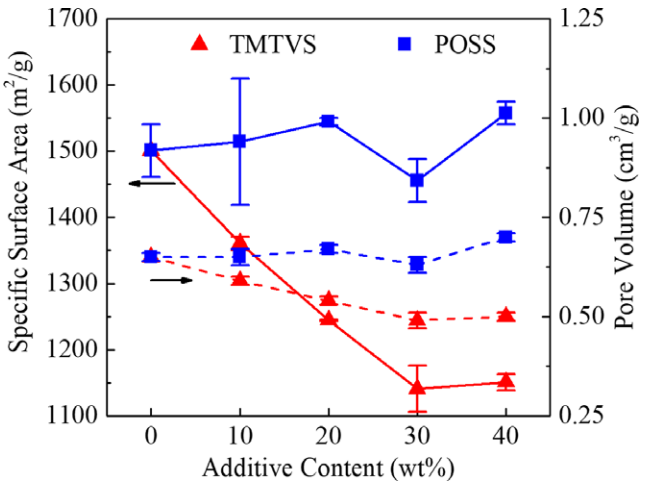

FIGURE 8 Specific surface area (solid lines) and pore volume (dashed lines) for the samples pyrolyzed at 1300°C [Color figure can be viewed at wileyonlinelibrary.com]

additions. SiC formation is not as significant in these samples compared to similar carbon-rich samples due to the water vapor injection between 500°C and 700°C. The water vapor encourages the formation of Si–O bonds at the expense of Si–C bonds within the samples, which results in increased SiO_2 formation and reduced SiC formation at higher pyrolysis temperatures.[8,9,19,20] After pyrolysis at 1400°C, the PSO and 30T samples show more extensive SiC formation. For the 30P sample, the onset of SiC formation is delayed until 1400°C, and the SiC diffraction peaks are much smaller than for either the PSO sample or the 30T sample. The formation of SiC within SiOC is through either the phase separation of the amorphous SiOC[5,9,18]:

$$2\mathrm{SiOC} \rightarrow \mathrm{SiO_2(amorphous)} + \mathrm{SiC}(\beta) + \mathrm{C} \quad (3)$$

or the carbothermal reduction of SiO_2:

$$\mathrm{SiO_2(amorphous)} + 3\mathrm{C} \rightarrow \mathrm{SiC}(\beta) + 2\mathrm{CO(g)} \uparrow \quad (4)$$

Considering that the mass loss from 1100°C to 1400°C is approximately 3 wt% for all the samples, forming only ~2.5 wt% SiC if following Equation (4), then the more dominant cause for SiC formation is through the phase separation of SiOC following Equation (3). This is further supported by the increased SiC formation for PSO and 30T between 1300°C and 1400°C, even though the samples experience no major change in the ceramic yield at the same temperatures.

Whether the amorphous halo in Figure 5 for the samples pyrolyzed at 1100°C is solely due to the SiOC phase or the nucleation of SiO_2 can be determined through the HF etching results. SiOC is highly resistant to leaching with HF, so only through phase separation and formation of SiO_2 nanodomains can SiOC be etched to cause mass loss.[35] For the PSO sample pyrolyzed at 1100°C, the mass loss after etching is 14% as shown in Figure 6. With the addition of TMTVS, the etching mass loss is slightly decreased, with most samples showing less than 10% mass loss. The incorporation of the POSS additive causes an increase in the etching mass loss for all the samples compared with the pure PSO. Thus, POSS is believed to encourage the nucleation of SiO_2 within SiOC at temperatures as low as 1100°C, attributed to its Si-containing cage molecular structure.

Increasing the pyrolysis temperature to 1300°C causes further etching mass loss for all the samples, due to further phase separation of SiOC as already discussed. For the

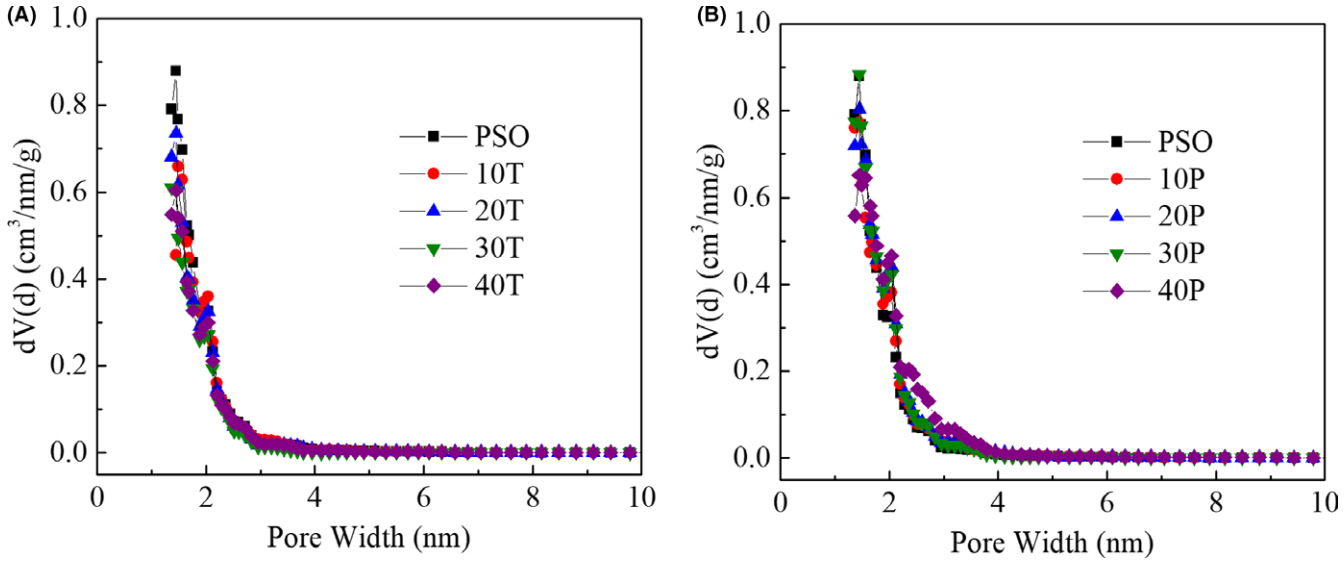

FIGURE 9 Pore size distributions of the (A) TMTVS and (B) POSS samples pyrolyzed at 1300°C [Color figure can be viewed at wile yonlinelibrary.com]

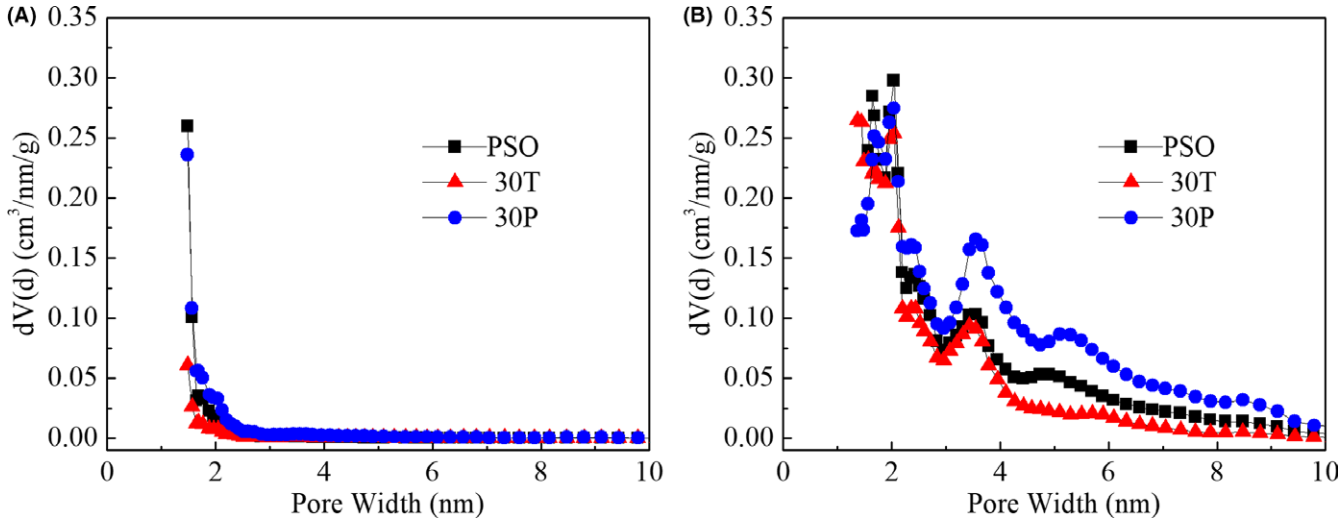

FIGURE 10 Pore size distributions after etching for PSO, 30T, and 30P pyrolyzed at (A) 1100°C and (B) 1400°C [Color figure can be viewed at wileyonlinelibrary.com]

TMTVS samples, the etching mass is less than that of the PSO or POSS samples and does not show any trend with the TMTVS content. This observation is consistent with the understanding that TMTVS is not conducive for SiO_2 nanocluster formation. The etching mass loss for the POSS samples is relatively constant for all the samples and close to the mass loss of the PSO samples.

3.4 | Specific surface area and pore size distribution

As shown in Figure 7, all the samples show a large adsorption volume at low relative pressures, followed by a relative constant adsorption volume at higher relative pressures; this adsorption behavior corresponds to the Type I isotherm, according to the IUPAC classification, which indicates that the samples are prominently microporous with only monolayer adsorption.[36] For the TMTVS samples, the adsorption volume at $P/P_o \sim 1$ steadily decreases as the TMTVS content increases, indicating a decrease in the total pore volume. For the samples with POSS additions, the adsorption volumes are almost the same as that of the PSO sample for the 10P, 20P, and 30P samples. With an increase of the POSS content to 40 wt%, however, the adsorption volume at relative pressures above 0.2 slightly increases compared to the other POSS samples, indicating that the mesopore volume for the 40P sample is greater than for any of the other samples with POSS.

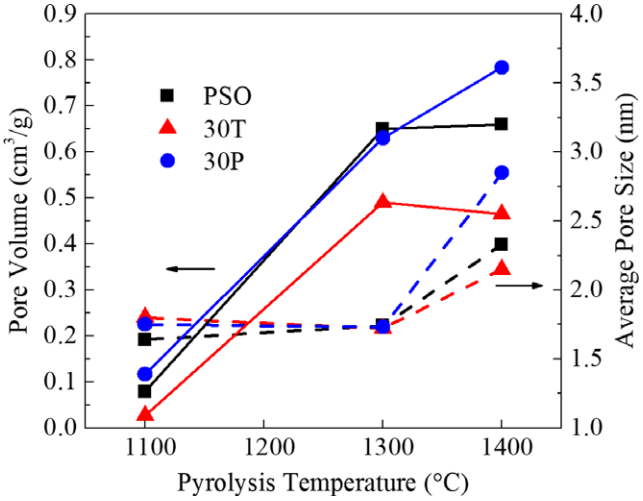

FIGURE 11 Pore volume (solid lines) and average pore size (dashed lines) for the PSO, 30T, and 30P samples at different pyrolysis temperatures [Color figure can be viewed at wileyonlinelibrary.com]

The results from nitrogen adsorption are shown in Figure 8. For the TMTVS samples, the specific surface area and total pore volume also decrease with increasing TMTVS content, from 1500.9 m^2/g and 0.65 cm^3/g, respectively, for the PSO sample to 1150.7 m^2/g and 0.50 cm^3/g, respectively, for the 40T sample. The reason for the negative effects of the TMTVS additive can be understood by considering the phase formation in Figure 5. At 1100°C, the samples with a higher TMTVS content produces more amorphous SiOC rather than forming SiO_2. As the temperature increases to 1300°C, the SiOC then phase separates, forming more SiC and less SiO_2 than the samples with a low TMTVS additive content. Thus, after etching, the samples with higher TMTVS amounts have less SiO_2 to generate pores and thus produce lower pore volumes. For the samples with the POSS additive, both the pore volume and specific surface area are largely independent of the additive content and produce slightly higher specific surface areas and similar pore volumes compared to the PSO sample.

The pore size distributions for the samples pyrolyzed at 1300°C after etching are shown in Figure 9. All the samples have similar pore sizes of < 2 nm and no large pores. For the pure PSO sample, the mode of the pore size distribution occurs at ~1.6 nm. The TMTVS samples show approximately the same pore size as the PSO sample, regardless of the TMTVS content, with the only significant difference in the pore concentration. Similarly, none of the POSS samples except for the 40P sample, which contains only slightly larger pores, show any significant changes in the pore size distribution compared to the PSO sample.

To understand the effect of pyrolysis temperature on the evolution of the SiO_2 nanodomains within the samples, pore size distributions are shown in Figure 10A,B, respectively, for the PSO, 30T, and 30P samples pyrolyzed at 1100°C and 1400°C. At 1100°C, the pore size distributions have only 1 mode at approximately 1.6 nm, similar to all of the samples pyrolyzed at 1300°C. Upon further heating to 1400°C, however, the pore size distributions begin to contain multiple modes as seen in Figure 9B. For PSO, the modes occur at ~1.8 nm, 3.5 nm, and 4.9 nm; similarly, the 30T sample has modes at ~1.8 nm and 4.9 nm, and the 30P sample has modes at ~1.8 nm, 3.9 nm, and 5.3 nm. Compared to the PSO, the 30T sample contains fewer pores larger than 4 nm, while the 30P sample contains a significantly larger volume of pores greater than 3 nm.

3.5 | Evolution of SiO_2 nanodomains

At low pyrolysis temperatures between 1100°C and 1300°C, the POSS and TMTVS additives have little influence on the resulting SiO_2 size, as seen in Figures 9 and 10A. Thus, the nucleation of SiO_2 nanodomains from the SiOC matrix is more dominant than their growth. To further study the effects of the TMTVS and POSS additives on the nucleation of SiO_2, or pores after etching, within the SiOC, the pore volume and pore size for the PSO, 30T, and 30P samples at different pyrolysis temperatures are plotted in Figure 11. At 1100°C, the 30P sample has a pore volume of 0.12 cm^3/g, approximately 1.5 times that of the PSO sample (0.079 cm^3/g), while the 30T sample only has a pore volume of 0.027 cm^3/g. Thus, the POSS additive facilitates the nucleation of SiO_2 within the SiOC at lower temperatures, as also evidenced by the etching mass loss in Figure 6. Increasing the pyrolysis temperature to 1300°C results in a significant increase in the pore volume for all 3 samples, and the PSO (0.66 cm^3/g) and 30P (0.78 cm^3/g) samples contain greater pore volumes than the 30T sample (0.47 cm^3/g). Further increasing the pyrolysis temperature to 1400°C results in almost no change in the pore volume for the PSO and 30T samples. However, the 30P sample continues to show increased pore volume upon heating from 1300°C to 1400°C.

In addition to the pore volume, the average pore size is also shown in Figure 11. At pyrolysis temperatures between 1100°C and 1300°C, the average pore size for all the PSO, 30T, and 30P samples is constant at ~1.7 nm. Upon further heating to 1400°C, all samples experience significant growth of the pores. Thus, the growth of the SiO_2 domains becomes more significant at temperatures above 1300°C. At 1400°C, the PSO and 30T samples have nearly the same pore size, 2.2 nm and 2.3 nm, respectively. However, the average pore size for the 30P sample is significantly greater at 2.9 nm. A possible explanation for the increase in pore volume and more significant growth in pore size for the 30P sample after pyrolysis at 1400°C is

that the more numerous SiO_2 domains in the 30P sample also have more inter-mixing with the SiOC matrix. Previous studies have found that etching SiOC ceramics with HF may unintentionally leach phases other than SiO_2. This removal is not due to the other phases reacting with HF, but rather due to the SiO_2 surrounding and encapsulating the other phases, and thus causing their physical removal when SiO_2 is removed.[8,24] It is possible that the SiO_2 domains within the 30P are more dispersed within the SiOC matrix and discrete SiOC, SiC, or graphitic species may be removed as well, causing a significant increase in pore volume and size.

From Figure 11, it is clear that the TMTVS additive more significantly affects the nucleation of SiO_2 within the SiOC and not the growth. For the homogeneous nucleation of SiO_2 in SiOC, there is a critical nuclei size required to overcome the interfacial energy of the surrounding matrix.[37,38] Given the small size of the TMTVS molecules, the majority of the SiO_2 nanodomains derived from the TMTVS are unlikely to be large enough to form stable nuclei. This would explain the deleterious effects of the TMTVS additive on the pore volume at all pyrolysis temperatures and lower etching mass loss; if the TMTVS ultimately contributes to more SiOC formation, there would be more SiC derived from the SiOC phase separation at higher temperatures following Equation (3), as evidenced in Figure 5.

4 | CONCLUSIONS

Tetramethyl-tetravinylcyclotetrasiloxane and POSS additives are successfully incorporated into the PSO matrix at the molecular level. The POSS additive significantly increases the SiOC ceramic yield and decreases the linear shrinkage after pyrolysis. It also leads to more SiO_2 nanodomains and slightly increases the specific surface area, up to 1557 m^2/g with a larger pore size of ~1.8 nm. Thus, POSS is an excellent additive in polymer derived porous SiOC due to its enhancement of thermal stability during the polymer-to-ceramic conversion, lowering of the SiO_2 nucleation temperature, and positive contribution to specific surface area and pore volume.

ACKNOWLEDGMENT

We acknowledge the financial support from National Science Foundation under grant number CMMI-1634325.

CONFLICT OF INTEREST

There are no conflicts to declare.

ORCID

Kathy Lu http://orcid.org/0000-0002-2135-6351

REFERENCES

1. Colombo P, Mera G, Riedel R, Soraru GD. Polymer-derived ceramics: 40 years of research and innovation in advanced ceramics. J Am Ceram Soc. 2010;93:1805–37.
2. Lu K. Porous and high surface area silicon oxycarbide-based materials-a review. Mater Sci Eng R Rep. 2015;97:23–49.
3. Greil P. Polymer derived engineering ceramics. Adv Eng Mater. 2000;2:339–48.
4. Colombo P. Engineering porosity in polymer-derived ceramics. J Eur Ceram Soc. 2008;28:1389–95.
5. Saha A, Raj R. Crystallization maps for SiCO amorphous ceramics. J Am Ceram Soc. 2007;90:578–83.
6. Saha A, Raj R, Williamson DL. A model for the nanodomains in polymer-derived SiCO. J Am Ceram Soc. 2006;89:2188–95.
7. Lu K, Erb D, Liu M. Thermal stability and electrical conductivity of carbon-enriched silicon oxycarbide. J Mater Chem C. 2016;4:1829–37.
8. Lu K, Li J. Fundamental understanding of water vapor effect on SiOC evolution during pyrolysis. J Eur Ceram Soc. 2016;36:411–22.
9. Li JK, Lu K. Highly porous SiOC bulk ceramics with water vapor assisted pyrolysis. J Am Ceram Soc. 2015;98:2357–65.
10. Narisawa M, Funabiki F, Iwase A, Wakai F, Hosono H. Effects of atmospheric composition on the molecular structure of synthesized silicon oxycarbides. J Am Ceram Soc. 2015;98:3373–80.
11. Sousa BF, Yoshida IVP, Ferrari JL, Schiavon MA. Silicon oxycarbide glasses derived from polymeric networks with different molecular architecture prepared by hydrosilylation reaction. J Mater Sci. 2013;48:1911–9.
12. Dibandjo P, Dire S, Babonneau F, Soraru GD. Influence of the polymer architecture on the high temperature behavior of SiCO glasses: a comparison between linear- and cyclic-derived precursors. J Non-Cryst Solids. 2010;356:132–40.
13. Dibandjo P, Dire S, Babonneau F, Soraru GD. New insights into the nanostructure of high-C SiOC glasses obtained via polymer pyrolysis. Glass Technol: Eur J Glass Sci Technol, Part A. 2008;49:175–8.
14. Hasik M, Wojcik-Bania M, Nyczyk A, Gumula T. Polysiloxane-POSS systems as precursors to SiCO ceramics. React Funct Polym. 2013;73:779–88.
15. Kolel-Veetil MK, Fears KP, Qadri SB, Klug CA, Keller TM. Formation of a crosslinked POSS network by an unusual hydrosilylation: thermo-oxidative stabilization of the α-cristobalite phase in its amorphous regions. J Polym Sci, Part A: Polym Chem. 2012;50:3158–70.
16. Yang D, Zhang W, Yao RL, Jiang BZ. Thermal stability enhancement mechanism of poly(dimethylsiloxane) composite by incorporating octavinyl polyhedral oligomeric silsesquioxanes. Polym Degrad Stab. 2013;98:109–14.
17. Wang X, Hu YA, Song L, Xing WY, Lu HD. Thermal degradation behaviors of epoxy resin/POSS hybrids and phosphorus-silicon synergism of flame retardancy. J Polym Sci, Part B: Polym Phys. 2010;48:693–705.

18. Li JK, Lu K, Lin TS, Shen FY. Preparation of micro-/mesoporous SiOC bulk ceramics. J Am Ceram Soc. 2015;98:1753–61.
19. Erb D, Lu K. Additive and pyrolysis atmosphere effects on polysiloxane-derived porous SiOC ceramics. J Eur Ceram Soc. 2017;37:4547–57.
20. Liang T, Li YL, Su D, Du HB. Silicon oxycarbide ceramics with reduced carbon by pyrolysis of polysiloxanes in water vapor. J Eur Ceram Soc. 2010;29:2677–82.
21. Janakiraman N, Aldinger F. Fabrication and characterization of fully dense Si-C-N ceramics from a poly (ureamethylvinyl) silazane precursor. J Eur Ceram Soc. 2009;29:163–73.
22. Martinez-Crespiera S, Ionescu E, Kleebe HJ, Riedel R. Pressureless synthesis of fully dense and crack-free SiOC bulk ceramics via photo-crosslinking and pyrolysis of a polysiloxane. J Eur Ceram Soc. 2011;31:913–9.
23. Ravikovitch PI, Neimark AV. Characterization of nanoporous materials from adsorption and desorption isotherms. Colloids Surf A. 2001;187:11–21.
24. Peña-Alonso R, Sorarù GD, Raj R. Preparation of ultrathin-walled carbon-based nanoporous structures by etching pseudo-amorphous silicon oxycarbide ceramics. J Am Ceram Soc. 2006;89:2473–80.
25. Anderson DR. Infrared, Raman, and ultraviolet spectroscopy. In: *Analysis of silicones*. Smith AL (ed). Malabar, FL: Robert E. Krieger Publishing Company Inc; 1983: pp. 257–79.
26. Liu GW, Kaspar J, Reinold LM, Graczyk-Zajac M, Riedel R. Electrochemical performance of DVB-modified SiOC and SiCN polymer-derived negative electrodes for lithium-ion batteries. Electrochim Acta. 2013;106:101–8.
27. Nyczyk-Malinowska A, Wojcik-Bania M, Gumula T, Hasik M, Cypryk M, Olejniczak Z. New precursors to SiCO ceramics derived from linear poly(vinylsiloxanes) of regular chain composition. J Eur Ceram Soc. 2014;34:889–902.
28. Hourlier D, Venkatachalam S, Ammar MR, Blum Y. Pyrolytic conversion of organopolysiloxanes. J Anal Appl Pyrolysis. 2017;123:296–306.
29. Camino G, Lomakin SM, Lageard M. Thermal polydimethylsiloxane degradation. Part 2. The degradation mechanisms. Polymer. 2002;43:2011–5.
30. Gibbons GJ, Holland D, Howes AP. Structure development in simple cross-linked organopolysiloxanes. J Sol-Gel Sci Technol. 1998;13:379–83.
31. Ku HH. Notes on use of propagation of error formulas. J Res Natl Bur Stand Sec C. 1966;70C:263–73.
32. Brequel H, Enzo S, Walter S, Sorarù GD, Badheka R, Babonneau F. Structure/property relationship in silicon oxycarbide glasses and ceramics obtained via the sol-gel method. J Metastable Nanocryst Mater. 2002;13:359–64.
33. Walter S, Soraru GD, Brequel H, Enzo S. Microstructural and mechanical characterization of sol gel-derived Si-O-C glasses. J Eur Ceram Soc. 2002;22:2389–400.
34. Soraru GD, Dallapiccola E, Dandrea G. Mechanical characterization of sol-gel-derived silicon oxycarbide glasses. J Am Ceram Soc. 1996;79:2074–80.
35. Soraru GD, Modena S, Guadagnino E, Colombo P, Egan J, Pantano C. Chemical durability of silicon oxycarbide glasses. J Am Ceram Soc. 2002;85:1529–36.
36. Sing KSW. Reporting physisorption data for gas solid systems - with special reference to the determination of surface-area and porosity. Pure Appl Chem. 1982;54:2201–18.
37. Yu L, Raj R. On the thermodynamically stable amorphous phase of polymer-derived silicon oxycarbide. Sci Rep. 2015;5:14550.
38. Varga T, Navrotsky A, Moats JL, Morcos RM, Poli F, Müller K, et al. Thermodynamically stable $Si_xO_yC_z$ polymer-like amorphous ceramics. J Am Ceram Soc. 2007;90:3213–9.

SUPPORTING INFORMATION

Additional supporting information may be found online in the Supporting Information section at the end of the article.

How to cite this article: Erb D, Lu K. Effect of additive structure and size on SiO_2 formation in polymer-derived SiOC ceramics. *J Am Ceram Soc*. 2018;101:5378–5388. https://doi.org/10.1111/jace.15876